# Microporosity Development of Single-Wall Carbon Nanohorn with Chemically Induced Coalescence of the Assembly Structure

**Cheol-Min Yang,*,† Daisuke Kasuya,‡ Masako Yudasaka,† Sumio Iijima,†,‡,§ and Katsumi Kaneko*,||**

*Japan Science and Technology Corporation, c/o NEC Corporation, 34 Miyukigaoka, Tsukuba 305-8501, Japan, Department of Material Science and Engineering, Faculty of Science and Technology, Meijo University, 1-501 Shiogamaguchi, Tempaku, Nagoya 468-8502, Japan, NEC Corporation, 34 Miyukigaoka, Tsukuba 305-8501, Japan, and Department of Chemistry, Faculty of Science, Chiba University, 1-33 Yayoi, Inage, Chiba 263-8522, Japan*

*Received: April 13, 2004; In Final Form: September 5, 2004*

Single-wall carbon nanohorns (SWNHs) with dahlia flowerlike structures were treated with $H_2SO_4$ and $H_2O_2$/$H_2SO_4$ mixture. The SWNH samples before and after acid treatment were characterized using a transmission electron microscopy (TEM), scanning electron microscopy (SEM), Raman spectroscopy, temperature-programmed desorption (TPD), and $N_2$ adsorption at 77 K. According to TEM and SEM observation, the SWNH bundles were coalesced after $H_2SO_4$ and $H_2O_2/H_2SO_4$ treatments, growing up to the bundle size of several micrometers. The Raman spectra provided evidence that the $H_2O_2/H_2SO_4$ treatment leads to intercalation of the $H_2SO_4$ molecule into interstitial spaces of individual SWNHs as well as defect formation by oxidation reaction. The $H_2O_2/H_2SO_4$ treatment also altered markedly the $N_2$ adsorption isotherms of SWNH from type II to type I, accompanied with an enhanced $N_2$ adsorption uptake at low relative pressure due to the development of microporosity. Heat treatment at 873 K on $H_2O_2/H_2SO_4$-treated SWNHs additionally increased the $N_2$ adsorption amount at the low relative pressure range. The $H_2O_2/H_2SO_4$ treatment remarkably increased the total surface area and micropore volume. In particular, micropore volume increased almost 5.5 times after $H_2O_2/H_2SO_4$ treatment and successive heat treatment (from 0.11 to 0.60 mL $g^{-1}$), whereas mesopore volume dramatically decreased (from 0.28 to 0.06 mL $g^{-1}$). Thereby micropore volume percent remarkably increased from 28 to 91%. The $H_2O_2/H_2SO_4$ treatment of SWNHs enhanced the microporosity due to increase not only of internal pore volume but also interstitial pore volume, which can be achieved by both opening of nanohorn particles and $H_2SO_4$ intercalation into the interstitial space between nanohorns. Moreover, the coalescence of SWNH assemblies by $H_2O_2/H_2SO_4$ treatment should transform the mesopores to micropores, and it decreases the external surface area.

## Introduction

Single-wall carbon nanotubes (SWNTs)[1] have gathered much attention from science and technology due to their novel properties and potential applications in nanotechnological fields.[2−5] Recently, a new SWNT-related material, which was named single-wall carbon nanohorns (SWNHs), was synthesized by Iijima et al.[6−9] SWNHs, which have high yield, high production rate, and high purity, can be prepared by $CO_2$ laser ablation of pure graphite at room temperature without any metal catalyst.[6] An individual tubule of SWNH has a diameter of about 2−3 nm with a length of 30−50 nm, and they form spherical assemblies of about 80 nm in diameter.[6] Such SWNH assemblies provide both microporosity and mesoporosity, which are governed by opening and assembling of nanohorns. Inner empty spaces of the individual tubule of SWNT-related materials could be available for gas adsorption and gas storage after the tube opening.[10,11] SWNT-related materials should provide a high surface area and high microporosity in order to use them in gas storage. According to the previous research reports, however, they do not show so high surface area and micropore volume, although SWNTs have the potential to improve the porosity.[12−14]

SWNHs have been proposed as a promising material for gas adsorption and storage.[10,11,15] However, as-grown SWNHs show low microporosity due to their closed hollow structures. The earlier study showed that heat treatment of SWNHs in $O_2$ opens almost perfectly their closed caps, and thereby highly microporous and mesoporous SWNHs are obtained.[16] SWNH assemblies should also have a high packing density to use them for gas storage; however, SWNHs opened in $O_2$ have a very low packing density.[16] Several studies of chemical intercalation of sulfuric acid ($H_2SO_4$) into graphite in the presence of hydrogen peroxide ($H_2O_2$) have been reported.[17,18] Moreover, according to previous studies, chemical oxidation by $H_2O_2/H_2SO_4$ treatment created the defects on the nanotube walls, accompanied by production of the oxygen-containing functional groups at the defect sites.[19−22]

In this study, the treatments with the $H_2O_2/H_2SO_4$ mixture at different ratios and successive heat treatment of dahlia-like

* To whom correspondence should be addressed C.-M. Yang. Present address: Center for Nanotubes and Nanostructured Composites, Sungkyunkwan University, Suwon 440-746, Republic of Korea. Fax: 82-31-290-5954. E-mail: cmyang1119@empal.com. K. Kaneko. Fax: 81-43-290-2788. E-mail: kaneko@pchem2.s.chiba-u.ac.jp.

† Japan Science and Technology Corp., c/o NEC Corp.

‡ Meijo University.

§ NEC Corp.

|| Chiba University.

10.1021/jp048391h CCC: $27.50 
Published on Web 10/23/2004

structured SWNHs were performed. Then, the influences of the treatments on the partial bundle structure and porosity changes of SWNH assemblies were investigated.

## Experimental Section

**Preparation and Chemical Treatment of SWNHs.** The dahlia-like structured SWNHs were synthesized with $CO_2$ laser ablation of a graphite target in Ar atmosphere (101 kPa).[6] The SWNHs of 100 mg were immersed without any further treatment and stirred (room temperature) in 100 mL mixtures of $H_2O_2$(30%)/$H_2SO_4$(97%) volume ratios of 0:10, 1:9, and 3:7 for 48 h, respectively. All precipitates were filtrated through a membrane filter and then washed with distilled water three times. After the samples were dried in air for 12 h at 348 K, the samples were heated in Ar at 523 K for 4 h. The samples treated with 0:10, 1:9, and 3:7 mixtures of $H_2O_2/H_2SO_4$ are donated as NH-(0:10), NH(1:9), and NH(3:7), respectively. The treated SWNH samples were heat-treated in inert gas atmosphere (Ar gas) for 1 h at 873 K with a heating rate of 100 K $min^{-1}$ in order to eliminate the intercalated molecules and introduced functional groups, which are donated as NH(0:10)-873, NH(1:9)-873, and NH(3:7)-873, respectively.

**Characterization of SWNHs.** Transmission electron microscope (TEM) images were obtained with a Topcon EM-002B instrument at 200 kV accelerating voltage. Field emission scanning electron microscopy (SEM) observations were carried out using a JSM6700F (JEOL) at 15 kV accelerating voltage. Raman spectroscopy measurements were performed at room temperature under ambient conditions, using a RM1000 microprobe Raman spectrometer (Renishaw). The Raman spectra were excited by the 514 nm wavelength of an Ar ion laser. Temperature-programmed desorption (TPD) analysis was carried out using TPD-MS4 (Shimadzu) in He flow (50 mL $min^{-1}$) to 1273 K with a heating rate of 10 K $min^{-1}$. The pore structures were determined by $N_2$ adsorption at 77 K using volumetric equipment (Quantachrome AS-1-MP) after preevacuation for 2 h at 423 K and $10^{-4}$ Pa. The pore structure parameters were obtained by the subtracting pore effect (SPE) method using high-resolution $\alpha_s$ plots constructed for the standard adsorption data on highly crystalline nonporous carbon black (Mitsubishi 4040B).[9,23]

## Results and Discussion

**Morphological Change of SWNHs with Chemical Treatment.** Figure 1 shows high-magnification TEM images of as-grown, $H_2SO_4$-, and $H_2O_2/H_2SO_4$-treated dahlia-SWNH assemblies. The TEM image of as-grown SWNHs shows the typical morphology of dahlia-like SWNH bundles (about 80 nm in bundle diameter; Figure 1a). The $H_2SO_4$ and $H_2O_2/H_2SO_4$ treatments for SWNHs dramatically change the arrangement of nanohorn bundles. SWNH bundles are coalesced as a result of $H_2SO_4$ and $H_2O_2/H_2SO_4$ treatments, and thereby they show very big bundle size (Figure 1b,d), which is expected to decrease the external surface area and the mesoporosity formed between SWNH bundles. Coalescence of SWNH bundles is independent of the presence of $H_2O_2$. Further heat treatment at 873 K on NH(0:10) and NH(1:9) does not give a pronounced change in morphology of SWNH bundles (Figure 1c,e). The individual nanohorn structure of SWNHs is preserved even after $H_2SO_4$ and $H_2O_2/H_2SO_4$ treatments (Figure 1f−h). Figure 2 presents low-magnification TEM images for as-grown and $H_2O_2/H_2SO_4$-treated SWNH assemblies. As-grown SWNH assemblies are formed by aggregation of spherical bundles (Figure 2a). The TEM image of as-grown SWNH assemblies shows many voids due to their large interbundle distance that is caused by weak interbundle interaction, and thereby they have the low packing density. On the contrary, the bundle size reaches several micrometers and the voids between bundles almost disappear as a result of $H_2O_2/H_2SO_4$ treatment on SWNH assemblies (Figure 2b,c), indicating higher packing density. Such an enhanced packing density should lead to a decrease of the external surface, mesopores, and macropores, as described later in $N_2$ adsorption results. Figure 3 shows SEM images for as-grown and $H_2SO_4$- and $H_2O_2/H_2SO_4$-treated SWNH assemblies. SEM images of as-grown SWNH assemblies show spherical bundle structure with a rough surface (Figure 3a). The protrusions with several nanometers in size exist on the spherical bundle surface due to individual nanohorns growing from the center of the bundle. On the other hand, spherical bundle structures of SWNHs disappear after $H_2SO_4$ and $H_2O_2/H_2SO_4$ treatments, and totally coalesced bundle structures are observed (Figure 3b,c). The surface is completely covered by the numerous protrusions whose size is several nanometers. TEM and SEM images clearly show that $H_2SO_4$ treatment without regard to the addition of $H_2O_2$ coalesces the SWNH bundles, and thereby it seems that the packing density of SWNH assemblies is considerably enhanced.

**Growth of Coalescence Structure due to Pseudointercalation and Charge-Transfer Interaction.** We used Raman spectroscopy to confirm the structural changes of the SWNHs which result from the acidic treatments. Figure 4 shows Raman spectra and the integrated intensity ratio of the D-band to G-band ($I_D/I_G$) of SWNHs samples. The G-band is related to the vibration mode in graphite-like carbon, whereas the D-band is attributed to the disordered $sp^2$ carbon by the defects in graphite sheets, respectively. The Raman spectrum of the as-grown SWNH assemblies shows two broad peaks centered at 1333 $cm^{-1}$ (D-band) and 1577 $cm^{-1}$ (G-band) with a similar intensity ($I_D/I_G = 1.01$), which is characteristic of dahlia-SWNH assemblies. All samples have D-band and G-band; however, their $I_D/I_G$ ratios are sensitively affected by the acidic treatment and the post-heat-treatment. The sample of NH(0:10) shows a lower $I_D/I_G$ ratio of 0.88, which should be associated with the crystallinity improvement by coalescence of SWNH bundles without defect formation due to the low oxidation ability of $H_2SO_4$ (concentrated $H_2SO_4$ at room temperature has low oxidation ability). On the contrary, the increase of the $I_D/I_G$ ratio (from 1.01 to 1.26) is observed after the $H_2O_2/H_2SO_4$ treatment, which should be attributed to an increment in the defect concentration of the nanohorn walls due to the liquid-phase oxidation. The post-heat-treatment of NH(1:9) additionally increases the $I_D/I_G$ ratio from 1.26 to 1.43, which comes from an increase in defects by release of carbon-based functional groups. On the other hand, heat treatment on NH(0:10) did not change the $I_D/I_G$ ratio, which is due to a small amount of carbon-based functional groups (as will be described later in TPD results). After $H_2SO_4$ treatment of SWNHs, Raman spectra show a decrease of $I_D/I_G$ value. However, SWNHs treated with mixture of $H_2O_2/H_2SO_4$ show increased $I_D/I_G$ value in Raman spectra. An increase of the $I_D/I_G$ value directly depends on defect formation on SWNH walls, that is, opening of a cap or sidewall of SWNH. Therefore, we suggest that $H_2O_2/H_2SO_4$ treatment can create defect sites on the cap and sidewall of SWNH, whereas $H_2SO_4$ treatment cannot create them. Additionally, the D-bands and G-bands of the $H_2O_2/H_2SO_4$-treated SWNH samples are upshifted in Raman frequency compared with those of as-grown SWNH sample. It is well-known that $H_2SO_4$ plays a role as electron acceptor in graphite−$H_2SO_4$ and nanotube−$H_2SO_4$ systems.[24,25] Previous study also showed that tangential

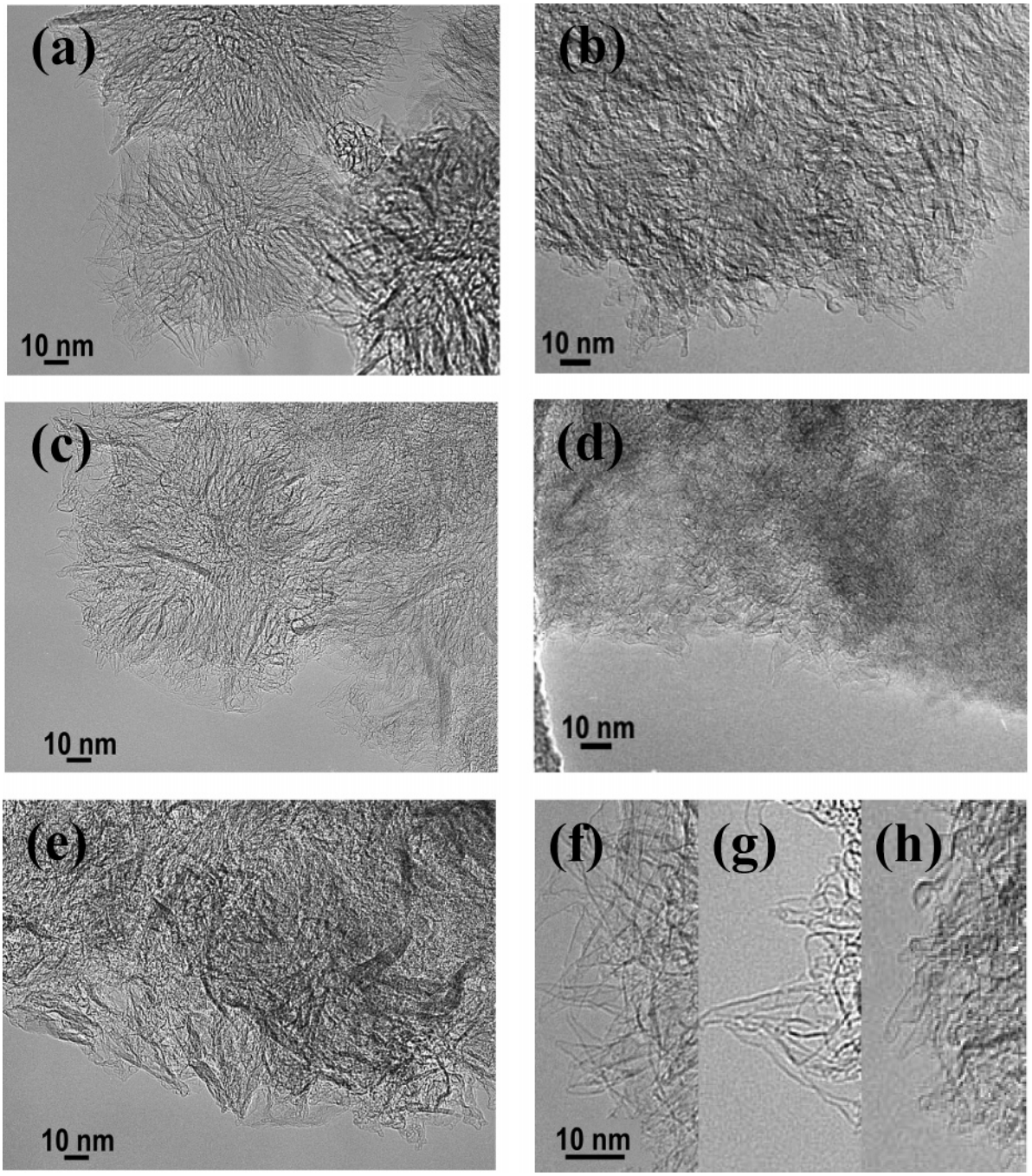


**Figure 1.** High-magnification TEM images of SWNH assemblies: (a, f) as-grown SWNHs; (b) NH(0:10); (c, g) NH(0:10)-873; (d) NH(1:9); (e, h) NH(1:9)-873.

modes in Raman spectra of SWNT and SWNH bundles reacted with the electron-acceptor dopants shift to higher frequency.[25−27] According to a previous report by Kang et al., chemical reaction between graphite and $H_2O_2/H_2SO_4$ was described as follows.[17]

$$H_2O_2 \rightarrow H_2O + O$$

$$24nC + mH_2SO_4 + 1/2O \rightarrow C_{24n}^{+}(HSO_4)^{-}(m-1)H_2SO_4 + 1/2H_2O$$

where $n$ and $m$ are the stage index and stoichiometric factor, respectively. Oxygen atoms decomposed from $H_2O_2$ oxidize the graphite, and then the oxidized graphite reacts with $HSO_4^-$. By analogy, we conjecture that the oxygen atoms can oxidize the SWNHs. Therefore, this upshift of Raman peak after $H_2O_2/H_2SO_4$ treatment should be explained in terms of the charge transfer by oxidation reaction between carbonaceous walls of SWNH and oxygen atoms (decomposed from $H_2O_2$). Moreover, splitting of the G-bands in Raman spectra has been often observed in graphite intercalation compounds of electron-acceptor type.[28−30] Therefore, the broadening of the G-bands of NH(1:9) and NH-(1:9)-873 should be ascribed to the intercalation of $H_2SO_4$ molecules. In contrast, $H_2SO_4$ treatment does not give such changes in Raman spectra. The Raman spectra provide decisive evidence that the $H_2O_2/H_2SO_4$ treatment leads to intercalation of $H_2SO_4$ molecules into interstitial spaces of individual SWNHs as well as defect formation due to the charge transfer (by oxidation reaction) between acid molecules and SWNH.

**Chemical Structural Change with Bundle Coalescence.** Figures 5 and 6 show TPD profiles of $CO_2$ and CO for SWNHs

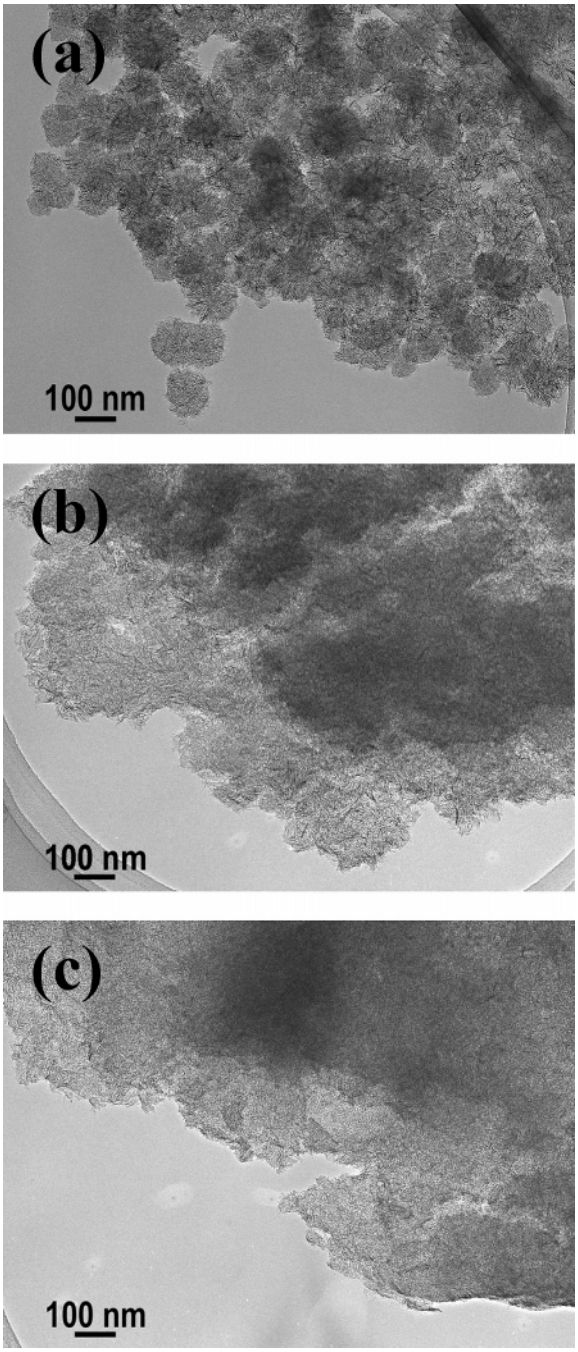


**Figure 2.** Low-magnification TEM images of SWNH assemblies: (a) as-grown SWNHs; (b) NH(1:9); (c) NH(1:9)-873.

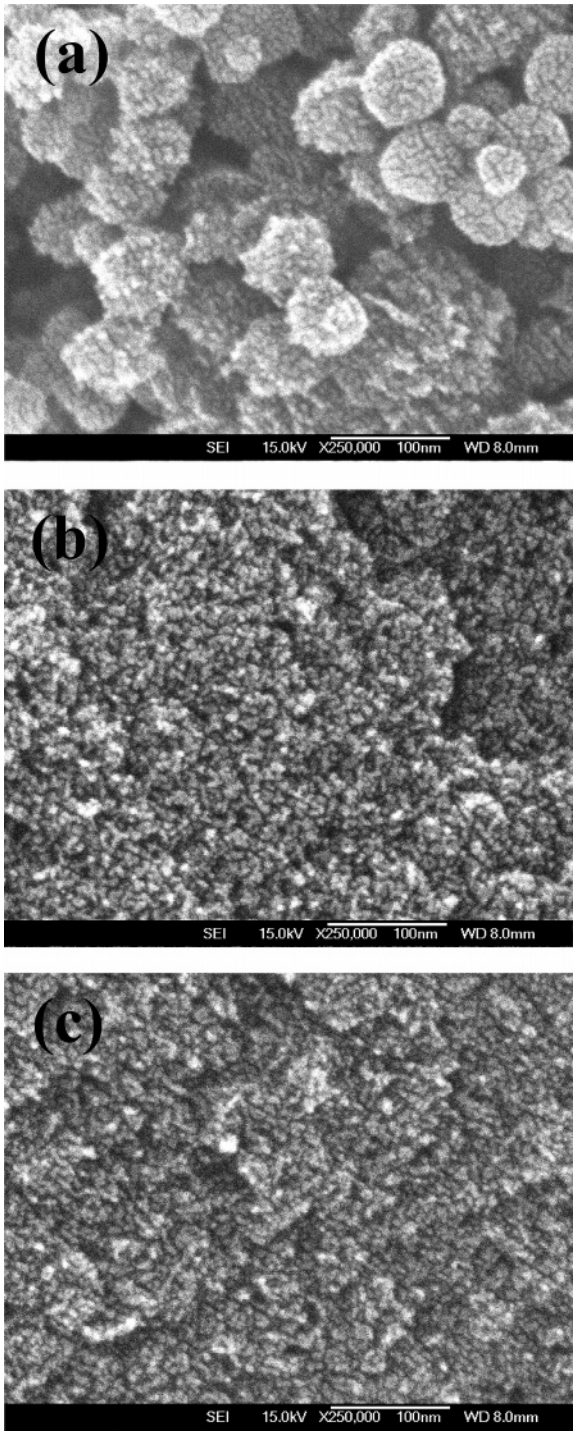


**Figure 3.** SEM images of SWNH assemblies: (a) as-grown SWNHs; (b) NH(0:10)-873; (c) NH(1:9)-873.

samples. The $CO_2$ comes from the decomposition of carboxylic acid, anhydride, and lactone groups, whereas CO comes from decomposition of phenolic, carbonyl, and quinone groups. The $CO_2$ TPD profile of as-grown SWNHs shows a broad peak in the temperature range of 600−1200 K (Figure 5). After $H_2O_2$/$H_2SO_4$ (1:9) treatment, marked changes are clearly observed in the $CO_2$ TPD profile. The $CO_2$ TPD profile of NH(1:9) has several overlapping peaks in the range of 400−1200 K, and its evolution rate considerably increases after $H_2O_2/H_2SO_4$ treatment. The maximum evolution rate of the $CO_2$ profile on NH(1:9) is shifted to lower temperature, which is associated with introduction of oxygen-containing functional groups having different thermal stability. The post-heat-treatment at 873 K after $H_2O_2/H_2SO_4$ treatment dramatically decreases the evolution rate in the $CO_2$ TPD profile. With regard to the CO TPD profile (Figure 6), as-grown SWNHs have a peak with maximum evolution rate at 950 K. On the contrary, the CO TPD profile of NH(1:9) has a broad peak in the range of 600−1273 K, and its evolution rate remarkably increases after the $H_2O_2/H_2SO_4$ treatment. The post-heat-treatment at 873 K after $H_2O_2/H_2SO_4$ treatment markedly decreases the evolution rate in the CO TPD profile. The amounts of $CO_2$ and CO evolved to 1273 K are summarized in Table 1. The desorbed amounts of $CO_2$ and CO due to oxygen-containing functional groups considerably increase from 3.6 to 14.5 wt % as a result of $H_2O_2/H_2SO_4$ treatment, whereas heat-treated SWNHs show much lower amounts of $CO_2$ and CO than even as-grown SWNHs. There-

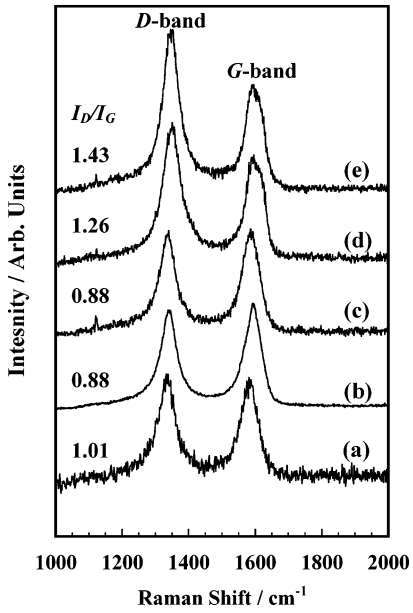


**Figure 4.** Raman spectra of SWHN assemblies: (a) as-grown SWNHs; (b) NH(0:10); (c) NH(0:10)-873; (d) NH(1:9); (e) NH(1:9)-873.

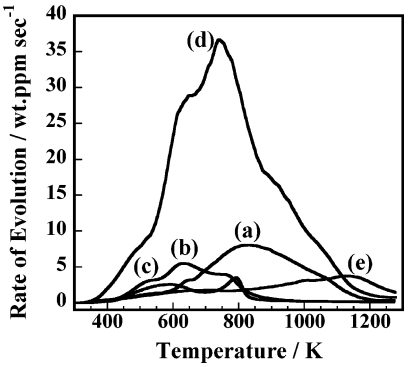


**Figure 5.** TPD profiles of $CO_2$ of SWHN assemblies: (a) as-grown SWNHs; (b) NH(0:10); (c) NH(0:10)-873; (d) NH(1:9); (e) NH(1:9)-873.

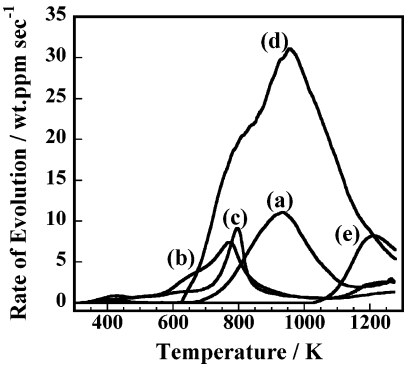


**Figure 6.** TPD profiles of CO of SWHN assemblies: (a) as-grown SWNHs; (b) NH(0:10); (c) NH(0:10)-873; (d) NH(1:9); (e) NH(1:9)-873.

fore, TPD results of $H_2O_2/H_2SO_4$-treated SWNHs clearly show that chemical oxidation by $H_2O_2/H_2SO_4$ treatment generates a large number of oxygen-containing functional groups as well as defects on the nanohorn walls and the post-heat-treatment at 873 K effectively eliminates such functional groups from defects. On the contrary, $H_2SO_4$-treated and post-heat-treated samples show lower amounts of $CO_2$ and CO than even as-grown SWNHs (Figures 5 and 6, Table 1). In general, after oxidation treatments of nanotube-related materials, oxygen-based

**TABLE 1: Amounts of $CO_2$ and CO Desorbed in TPD Analysis up to 1273 K**

| sample | $CO_2$ (mmol g$^{-1}$) | CO (mmol g$^{-1}$) | total amt ($CO_2$ + CO; wt %) |
|---|---|---|---|
| as-grown SWNHs | 0.4 | 0.6 | 3.6 |
| NH(0:10) | 0.2 | 0.4 | 2.0 |
| NH(0:10)-873 | 0.1 | 0.3 | 1.5 |
| NH(1:9) | 1.8 | 2.4 | 14.5 |
| NH(1:9)-873 | 0.3 | 0.3 | 1.8 |

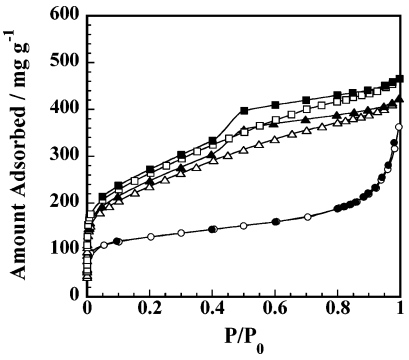


**Figure 7.** $N_2$ adsorption isotherms (77 K) of $H_2SO_4$-treated SWNH assemblies. The open and solid symbols indicate adsorption and desorption branches, respectively: ○, as-grown SWNHs; △, NH(0:10); □, NH(0:10)-873.

functional groups are present in defects. Therefore, differences of evolution amounts in CO and $CO_2$ TPD profiles between $H_2SO_4$-treated and $H_2O_2/H_2SO_4$-treated samples give information about the defect concentration on SWNHs. The $H_2O_2/H_2SO_4$-treated sample shows an increased evolution amount in CO and $CO_2$ TPD profiles, whereas the $H_2SO_4$-treated sample shows a decreased evolution amount in them. This also indicates that $H_2O_2/H_2SO_4$ treatment opened the cap or sidewall of SWNH, whereas $H_2SO_4$ treatment did not open them, which are in good agreement with Raman results.

**Microporosity Development with Bundle Coalescence.** Figure 7 presents $N_2$ adsorption isotherms of as-grown and $H_2SO_4$-treated SWNH assemblies. The $N_2$ adsorption isotherm of as-grown SWNHs is of type II in IUPAC classification without adsorption hysteresis. As-grown SWNHs show gradual uptake of $N_2$ at the medium $P/P_0$ and also show predominant adsorption of $N_2$ at the higher $P/P_0$, which are associated with multilayer adsorption on the external surface and macropores. The $N_2$ adsorption of as-grown SWNHs at low $P/P_0$ almost occurs in interstitial pores due to the closed structure of individual nanohorns.[9] On the contrary, the $N_2$ adsorption isotherms of NH(0:10) and NH(0:10)-873 are an intermediate shape between types I and II without steep adsorption uptake at high $P/P_0$, although they exhibit hysteresis loops. The $N_2$ adsorption isotherm of NH(0:10) has gradual uptake at medium $P/P_0$ range, which is associated with adsorption on macropores and/or external surfaces. $H_2SO_4$-treated SWNHs exhibit enhanced adsorption uptake of $N_2$ below $P/P_0 = 0.1$, indicating further development of micropores. Such an enhanced $N_2$ adsorption comes from the micropores produced by coalescence of SWNH bundles, as evidenced in the TEM and SEM images (Figures 1 and 3). The post-heat-treatment at 873 K on NH(0:10) slightly increases the $N_2$ adsorption amount. The $N_2$ adsorption isotherms (77 K) of SWNHs treated with a mixture of $H_2O_2/H_2SO_4$ volume ratio of 1:9 are shown in Figure 8. After $H_2O_2/H_2SO_4$ treatment, $N_2$ adsorption isotherm changes to type I with a steep uptake at lower $P/P_0$ and long plateau at higher $P/P_0$, which are associated with the presence of uniform microporosity and a small amount

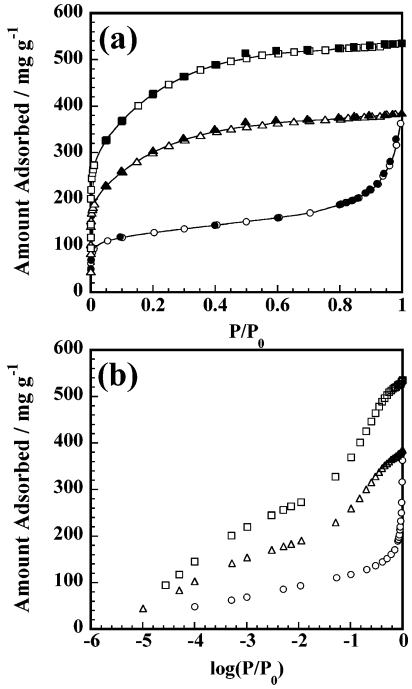


**Figure 8.** (a) $N_2$ adsorption isotherms (77 K) of SWHN assemblies treated with mixture of $H_2O_2/H_2SO_4$ volume ratios of 1:9 for 48 h. (b) $N_2$ adsorption isotherms in logarithmic scale. The open and solid symbols indicate adsorption and desorption branches, respectively: ○, as-grown SWNHs; △, NH(1:9); □, NH(1:9)-873.

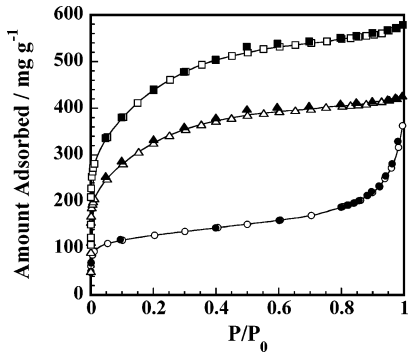


**Figure 9.** $N_2$ adsorption isotherms (77 K) of SWHN assemblies treated with mixture of $H_2O_2/H_2SO_4$ volume ratios of 3:7 for 48 h. The open and solid symbols indicate adsorption and desorption branches, respectively: ○, as-grown SWNHs; △, NH(3:7); □, NH(3:7)-873.

of external surfaces, respectively. Such a change in the isotherm type is essentially important to donate interfacial characteristics to SWNHs. This result strongly demonstrates that SWNH bundles are efficiently coalesced through the $H_2O_2/H_2SO_4$ treatment, as shown in the results of TEM and SEM observation. The $N_2$ adsorption amount of NH(1:9) below $P/P_0 = 0.1$ increases remarkably compared with that of as-grown SWNHs, indicating an intensive enhancement of adsorbent−adsorbate interaction due to the development of micropores. The post-heat-treatment at 873 K additionally increases the $N_2$ adsorption amount at lower $P/P_0$ range without change of the isotherm type (Figure 8a). Their $N_2$ adsorption isotherms of the $\log(P/P_0)$ axis are also shown in Figure 8b to show the detailed adsorption in micropores. Enhanced adsorption amounts of $N_2$ at low $P/P_0$ are clearly observed after acid treatment and post-heat-treatment. Figure 9 shows $N_2$ adsorption isotherms of SWNHs treated with a mixture of $H_2O_2/H_2SO_4$ volume ratio of 3:7. The samples of NH(3:7) and NH(3:7)-873 show a tendency similar to the 1:9 samples, except the $N_2$ uptake amount near $P/P_0 = 1$ slightly

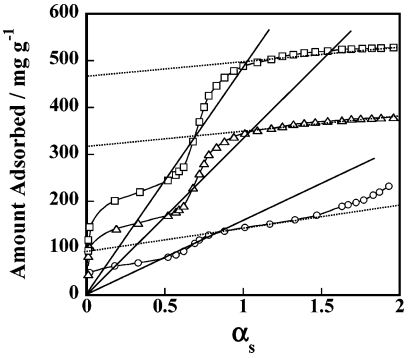


**Figure 10.** $\alpha_s$ plots of the $N_2$ adsorption isotherms (77 K) on SWHN assemblies treated with mixture of $H_2O_2/H_2SO_4$ volume ratios of 1:9 for 48 h: ○, as-grown SWNHs; △, NH(1:9); □, NH(1:9)-873.

increases. The post-heat-treatment at 873 K after $H_2O_2/H_2SO_4$ treatment (both 1:9 and 3:7) dramatically increases the $N_2$ adsorption amount, whereas the $N_2$ adsorption amount enhanced by heat treatment after $H_2SO_4$ treatment is not notable.

Figure 10 shows high-resolution $\alpha_s$ plots for $N_2$ adsorption isotherms of as-grown SWNHs, NH(1:9), and NH(1:9)-873 at 77 K. The SPE method using a $\alpha_s$ plot has been used as a very effective method for porosity evaluation. The slopes of solid and dotted lines give information about the total and external surface areas, respectively. The micropore volume was calculated from the ordinate intercept of the dotted line. The upward deviation due to the monolayer adsorption on the micropore walls is observed at the low-$\alpha_s$ region. The $H_2O_2/H_2SO_4$ treatment significantly enhances the upward deviation due to development of microporosity. The pore structure parameters of the samples obtained by the SPE method using the high-resolution $\alpha_s$ plots are summarized in Table 2. The mesopore volume was obtained by subtracting the micropore volume from the total pore volume which is determined from the adsorbed $N_2$ amount at $P/P_0 = 0.98$. According to the results by Bekyarova et al., SWNH assemblies compressed by successive compression with applying a high pressure of 50 MPa after dispersion in ethanol show a micropore volume of 0.20 mL $g^{-1}$, a mesopore volume of 0.32 mL $g^{-1}$, and a total surface area of 590 $m^2$ $g^{-1}$.[31] The $H_2SO_4$-treated SWNHs have very similar pore structure parameters with compactly packed SWNH assemblies after the compression. This result strongly suggests that the porosity change through this $H_2SO_4$ treatment originates from the increase of the packing density with the coalescence of SWNH bundles. Therefore, the empty inner spaces of individual nanohorns do not contribute to the porosity increase; the $H_2SO_4$ treatment binds SWNH bundles to each other without opening each SWNH particle. Heat treatment after $H_2SO_4$ treatment does not give pronounced changes in porosity. The $H_2O_2/H_2SO_4$ (1:9) treatment remarkably increases the total surface area and micropore volume. In particular, micropore volume increases almost 4 times after the $H_2O_2/H_2SO_4$ (1:9) treatment, whereas the mesopore volume dramatically decreases from 0.28 to 0.06 mL $g^{-1}$. The $H_2O_2/H_2SO_4$ treatment is efficient for developing the microporosity of SWNH assemblies, which provide the quantitative information on the opening of SWNHs. Furthermore, micropore volume percent remarkably increases after $H_2O_2/H_2SO_4$ (1:9) treatment from 28 to 87%. The post-heat-treatment at 873 K after $H_2O_2/H_2SO_4$ treatment additionally increases the micropore volume (to about 46%). NH(1:9)-873 shows very high values of specific surface area of 1015 $m^2$ $g^{-1}$ and micropore volume of 0.60 mL $g^{-1}$, whereas it shows a very low value of mesopore volume of 0.06 mL $g^{-1}$,

**TABLE 2: Pore Structure Parameters of SWNH Samples Determined by SPE Method**

| sample | total surface area ($m^2\ g^{-1}$) | external surface area ($m^2\ g^{-1}$) | total pore vol ($mL\ g^{-1}$) | micropore vol ($mL\ g^{-1}$) | mesopore vol ($mL\ g^{-1}$) | micropore vol % |
|---|---|---|---|---|---|---|
| as-grown SWNHs | 308 | 108 | 0.40 | 0.11 | 0.29 | 28 |
| NH(0:10) | 628 | 342 | 0.51 | 0.22 | 0.29 | 43 |
| NH(0:10)-873 | 632 | 213 | 0.57 | 0.20 | 0.37 | 35 |
| NH(1:9) | 703 | 61 | 0.47 | 0.41 | 0.06 | 87 |
| NH(1:9)-873 | 1015 | 48 | 0.66 | 0.60 | 0.06 | 91 |
| NH(3:7) | 774 | 77 | 0.52 | 0.43 | 0.09 | 83 |
| NH(3:7)-873 | 1048 | 98 | 0.71 | 0.60 | 0.11 | 85 |

which results in a high micropore volume percent of 91%. The post-heat-treatment at 873 K leads to the development of the microporosity of SWNH assemblies without a change of the mesopore structures. This can be explained as follows. Intercalated molecules and introduced functional groups block the micropores. Therefore, deintercalation of the intercalated molecules and elimination of the functional groups through the post-heat-treatment at 873 K open the blocked pores, and thereby microporosity additionally increases. SWNHs treated with a 3:7 mixture of $H_2O_2/H_2SO_4$ do not show further significant changes in the porosity compared with 1:9 samples.

**Chemical Treatment as Donation Method of High Microporosity to SWNH.** The earlier study showed that heat treatment of SWNHs in $O_2$ at 693 K opens almost perfectly SWNHs, and thereby 0.47 mL $g^{-1}$ of the micropore volume, 1006 $m^2\ g^{-1}$ of the specific surface area, and low micropore volume percent of 42% are obtained; only opening SWNH particles cannot give a highly great microporosity.[16] Therefore, it is necessary to control the interstitial pores as well as internal pores in order to obtain more highly porous SWNH assemblies. Highly microporous SWNH samples prepared in this study are likely to be obtained by controlling two kinds of pores. The interstitial pore can be formed at the spaces both between individual tubules and between spherical bundles. Therefore, the intercalation of $H_2SO_4$ into narrow interstitial spaces results in an increase of interstitial micropore volume. Moreover, coalescence of SWNH bundles should produce interstitial pores between the SWNH bundles. The newly produced pores should contribute to the microporosity, and they should lead to the decrease of the mesoporosity. Namely, the coalescence of SWNH bundles after the $H_2O_2/H_2SO_4$ treatment should transform the mesopores to micropores, and it decreases the external surface area due to growth of large assemblies of the SWNH bundles. Although thermally oxidized SWNHs at oxidizing gases show the enhanced microporosity, which should be associated with increase of internal pore volume only by the opening of closed nanohorns, chemical treatment using $H_2O_2/H_2SO_4$ provides high microporosity to SWNHs through control of both of interstitial and internal pore structures.

## Conclusions

Nanoporous materials for application in supercritical gas storage have a serious issue of how to develop the microporosity and reduce meso- and macroporosities. This issue is resolved with the simple chemical treatment proposed in this work. The $H_2O_2/H_2SO_4$ treatment considerably affects both the microporosity and mesoporosity of SWNHs. The $H_2O_2/H_2SO_4$ treatment for SWNHs gives three desirable effects for application as energy storage materials: (1) The $H_2O_2/H_2SO_4$ treatment increases the internal pores through opening the capped SWNHs by liquid-phase oxidation, (2) it increases the interstitial pores by the intercalation of $H_2SO_4$ in the presence of $H_2O_2$, and (3) it transforms mesoporosity to microporosity by the coalescence of SWNH bundles, and thereby micropore volume percent increases from 28 to 91%. Highly microporous SWNH assemblies with a small amount of external surfaces and mesopores were successfully prepared by the simple chemical method. Chemical oxidation effect by $H_2O_2/H_2SO_4$ treatment on nanotubes is well-known. Nevertheless, it should be stressed that the coalescence of SWNH bundles and the opening of SWNH occur at the same time, although it is not clear how the coalescence of SWNH bundles is brought about through the $H_2SO_4$ or $H_2O_2/H_2SO_4$ treatments. This chemical treatment provides an interesting possibility for attaining the high packing density which is essentially important in the application of SWNHs. We expect that this advanced material with high microporosity due to the proposed chemical treatment could give new dreams in science and technologies.

**Acknowledgment.** We thank the Japan Science and Technology Corp. for supporting this International Cooperative Research Project.

## References and Notes

(1) Iijima, S.; Ichihashi, T. *Nature* **1993**, *363*, 603.

(2) Dillon, A. C.; Jones, K. M.; Bekkedahl, T. A.; Kiang, C. H.; Bethune, D. S.; Heben, M. S. *Nature* **1997**, *386*, 377.

(3) Rinzler, A. G.; Hafner, J. H.; Nikolaev, P.; Lou, L.; Kim, S. G.; Tomanek, D.; Nordlander, P.; Colbert, D. T.; Smalley, R. E. *Science* **1995**, *269*, 1550.

(4) Niu, C.; Sichel, E. K.; Hoch, R.; Moy, D.; Tennent, H. *Appl. Phys. Lett.* **1997**, *70*, 1480.

(5) An, K. H.; Kim, W. S.; Park, Y. S.; Lim, I. S.; Bae, D. J.; Lee, S. M.; Choi, Y. C.; Lee, Y. H. *Adv. Mater.* **2001**, *13*, 497.

(6) Iijima, S.; Yudasaka, M.; Yamada, R.; Bandow, S.; Suenaga, K.; Kokai, F.; Takahashi, K. *Chem. Phys. Lett.* **1999**, *309*, 165.

(7) Bandow, S.; Kokai, F.; Takahashi, K.; Yudasaka, M.; Qin, L. C.; Iijima, S. *Chem. Phys. Lett.* **2000**, *321*, 514.

(8) Nisha, J. A.; Yudasaka, M.; Bandow, S.; Kokai, F.; Takahashi, K.; Iijima, S. *Chem. Phys. Lett.* **2000**, *328*, 381.

(9) Murata, K.; Kaneko, K.; Kokai, F.; Takahashi, K.; Yudasaka, M.; Iijima, S. *Chem. Phys. Lett.* **2000**, *331*, 14.

(10) Murata, K.; Kaneko, Kanoh, H.; Kasuya, D.; Takahashi, K.; Kokai, F.; Yudasaka, M.; Iijima, S. *J. Phys. Chem. B* **2002**, *106*, 11132.

(11) Bekyarova, E.; Murata, K.; Yudasaka, M.; Kasuya, D.; Iijima, S.; Tanaka, H.; Kanoh, H.; Kaneko, K. *J. Phys. Chem. B* **2003**, *107*, 4681.

(12) Eswaramoorthy, M.; Sen, R.; Rao, C. N. R. *Chem. Phys. Lett.* **1999**, *304*, 207.

(13) Du, W.; Wilson, L.; Ripmeester, J.; Dutrisac, R.; Simard, B.; Denommee, S. *Nano Lett.* **2002**, *2*, 343.

(14) Yang, C. M.; Kanoh, H.; Kaneko, K.; Yudasaka, M.; Iijima, S. *J. Phys. Chem. B* **2002**, *106*, 8994.

(15) Murata, K.; Hirahara, K.; Yudasaka, M.; Iijima, S.; Kasuya, D.; Kaneko, K. *J. Phys. Chem. B* **2002**, *106*, 12668.

(16) Murata, K.; Kaneko, K.; Steele, W. A.; Kokai, F.; Takahashi, K.; Kasuya, D.; Hirahara, K.; Yudasaka, M.; Iijima, S. *J. Phys. Chem. B* **2001**, *105*, 10210.

(17) Kang, F.; Leng, Y.; Zhang, T.-Y. *J. Phys. Chem. Solids* **1996**, *57*, 889.

(18) Tryba, B.; Przepiorski, J.; Morawski, A. W. *Carbon* **2002**, *41*, 2013.

(19) Kuznetsova, A.; Mawhinney, D. B.; Naumenko, V.; Yates, J. T., Jr.; Liu, J.; Smalley, R. E. *Chem. Phys. Lett.* **2000**, *321*, 292.

(20) Kuznetsova, A.; Popova, I.; Yates, J. T., Jr.; Bronikowski, M. J.; Huffman, C. B.; Liu, J.; Smalley, R. E.; Hwu, H. H.; Chen, J. G. *J. Am. Chem. Soc.* **2001**, *123*, 10699.

(21) Li, X.; Niu, J.; Zhang, J.; Li, H.; Liu, Z. *J. Phys. Chem. B* **2003**, *107*, 2453.

(22) Zhang, J.; Zou, H.; Qing, Q.; Yang, Y.; Li, Q.; Liu, Z.; Guo, X.; Du, Z. *J. Phys. Chem. B* **2003**, *107*, 3712.

(23) Yang, C. M.; Kaneko, K.; Yudasaka, M.; Iijima, S. *Nano Lett.* **2002**, *2*, 385.

(24) Henning, G. R. *Prog. Inorg. Chem.* **1959**, *1*, 125.

(25) Sumanasekera, G. U.; Allen, J. L.; Fang, S. L.; Loper, A. L.; Rao, A. M.; Eklund, P. C. *J. Phys. Chem. B* **1999**, *103*, 4292.

(26) Rao, A. M.; Eklund, P. C.; Bandow, S.; Thess, A.; Smalley, R. E. *Nature* **1997**, *388*, 257.

(27) Bandow, S.; Rao, A. M.; Sumanasekera, G. U.; Eklund, P. C.; Kokai, F.; Takahashi, K.; Yudasaka, M.; Iijima, S. *Appl. Phys. A* **2000**, *71*, 561.

(28) Dresselhaus, M. S.; Dresselhaus, G. *Adv. Phys.* **1981**, *30*, 139.

(29) Chieu, T. C.; Dresselhaus, M. S.; Endo, M. *Phys. Rev. B* **1982**, *26*, 5867.

(30) Gupta, V.; Nakajima, T.; Ohzawa, Y.; Zemva, B. *J. Fluorine Chem.* **2003**, *120*, 143.

(31) Bekyarova, E.; Kaneko, K.; Yudasaka, M.; Murata, K.; Kasuya, D.; Iijima, S. *Adv. Mater.* **2002**, *14*, 973.